Contents list available at IJRED website

International Journal of Renewable Energy Development

Journal homepage: https://ijred.undip.ac.id

Research Article

Investigation of the Impact of Large-Scale Wind Power and Solar Power Plants on a Vietnamese Transmission Network

Ngo Minh Khoa[a], Nguyen Thi Hai Van[b], Le Kim Hung[c], Doan Anh Tuan[c*]

[a]*Faculty of Engineering and Technology, Quy Nhon University, Quy Nhon city, Vietnam*

[b]*The University of Danang - University of Technology and Education, Da Nang city, Vietnam*

[c]*The University of Danang - University of Science and Technology, Da Nang city, Vietnam*

Abstract. Integrating wind power and solar power plants into a power system has significantly grown over the past decade and is expected to grow to unprecedented levels in the coming years. In Vietnam, much large-scale wind power and solar power plants have been built and connected to the power system in recent years. To investigate and evaluate the impact of these power plants on system power operation, the 110kV power transmission network of Binh Dinh province in Vietnam is used in this paper. In the system, the Phuong Mai 3 wind power plant with a capacity of 21MW, the Fujiwara solar power plant with a peak capacity of 50MWp, and the Cat Hiep solar power plant with a peak capacity of 49.5MWp are modeled by using the PSS/E software to simulate and analyze their impacts on power system stability of the 110kV transmission network in Binh Dinh province, Vietnam. Besides, the control strategies of these power plants are also established to investigate their impacts on the network. In addition, this paper proposes three typical scenarios for the wind power and solar power plants in the system. For each scenario, the grid's operating parameters such as voltage variations and frequency variations are acquired for analyzing and evaluating their impacts on the frequency and voltage variations of the network. The simulation results show that the 110kV power transmission network remains in a stable operation mode after the fault scenarios for the wind and solar power plants. Furthermore, these simulation results provide some guidance for the actual operation.

Keywords: Fault scenario, Frequency variation, Renewable resource, Transmission network, Voltage variation

Received: 3rd January 2022; Revised: 24th May 2022; Accepted: 1st June 2022; Available online: 20th June 2022

1. Introduction

In the shortage of resources from coal and minerals, hydropower plants and thermal power plants are also becoming increasingly saturated. The development of renewable resources is being encouraged by the Vietnamese government. Based on that, the development of wind power plants and solar power plants in golden fields is being promoted strongly. Investors are building wind turbines and solar farms that are skyrocketing production capacity in these areas, typically in Ninh Thuan, Binh Thuan, Binh Dinh provinces, etc. That makes the transmission lines and the power distribution of the dispatching units to be quite difficult. To solve the pressing problems at present, according to Electricity of Vietnam (EVN) at the time in August 2020, 113 solar and wind projects with a total capacity of 5,700MW allow for the release of concentrated capacity in most of the provinces of Ninh Thuan, Binh Thuan, and Binh Dinh in Vietnam (Dai *et al.* 2020). Thus, the amount of power energy transmitted to the grid, the problem of the line overload is needed to solve, responded to the practical amount of capacity for power consumption (Ullah *et al.* 2022). In addition to the positive factors, the large-scale wind and solar power plants integrated into the power system can cause many difficulties and challenges for the power system operation (Denholm *et al.* 2011; Hu *et al.* 2021; Impram *et al.* 2020). The main reason is the uncertain nature, which changes rapidly according to the weather, climate, and natural characteristics of each region (Fant *et al.* 2016; Jasemi *et al.* 2016; Khoa *et al.* 2018). Therefore, during the overheated development period for grid-connected renewable energy projects on a large scale at present, the impact analysis of large-scale wind power and solar power plants on the Vietnamese transmission network is studied by many researchers. Several papers are related works to this paper (Abbas *et al.* 2020; Ameur *et al.* 2019; Cheng *et al.* 2015; Djamel *et al.* 2016; Kim *et al.* 2011; Wu *et al.* 2016) as follows:

The work (Ameur *et al.* 2019) presented a methodology for identifying and overcoming technical challenges due to the intermittent nature of renewable resources. The PSS/E software simulation tool was applied in the work for

* Corresponding author:
Email: datuan@dut.udn.vn (D. A. Tuan)

https://doi.org/10.14710/ijred.2022.43879
ISSN: 2252-4940/© 2022.The Author(s). Published by CBIORE

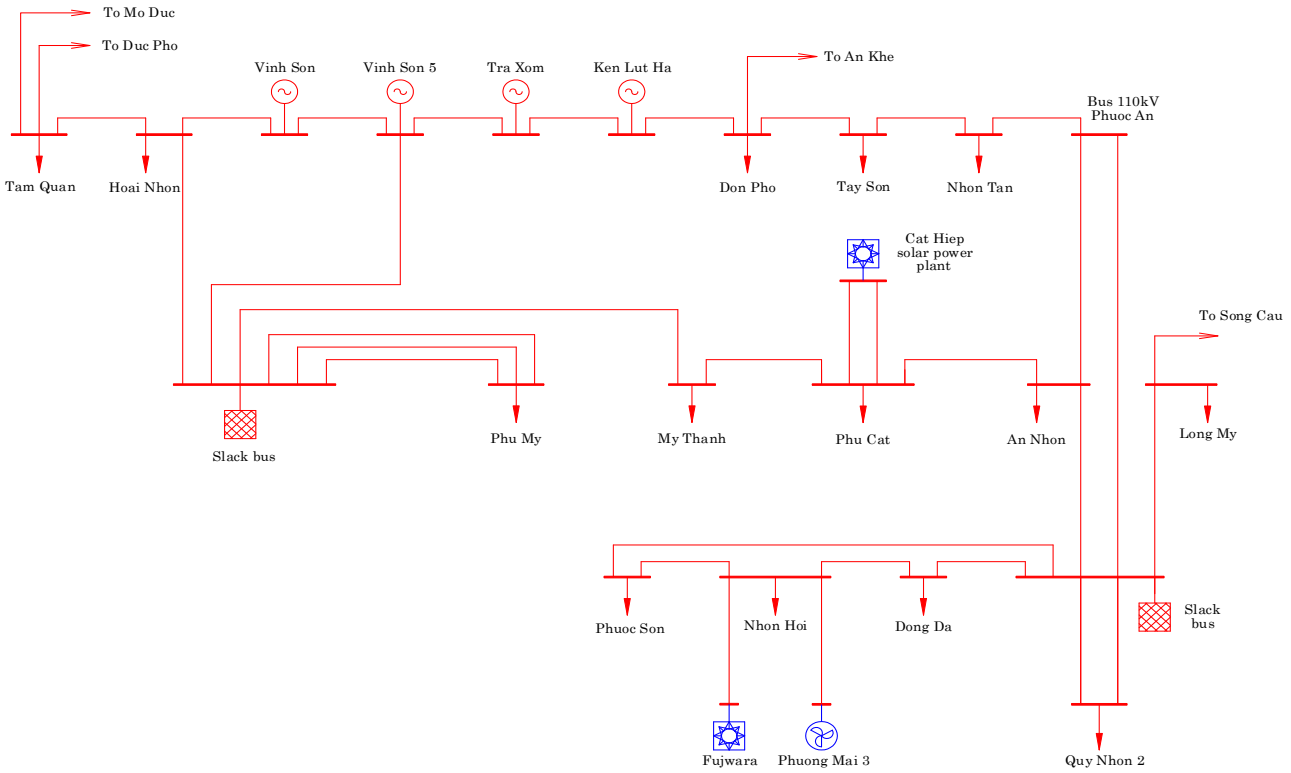

Fig. 1 The single diagram of 110 kV network Binh Dinh province

carrying out power flow analysis on the network's lines, bus bars, and transformers. The authors Abbas *et al.* 2020 addressed power quality problems that have arisen after integrating large-scale wind power plants into weak transmission grids. A recovery of significant active power deficits caused by the wake effect via increasing hub height of wind turbines was proposed. The work (Kim *et al.* 2011) presented modeling and impact analysis of wind farms in Jeju island power system, which was made of wind farms, a current source-type high-voltage, direct current (HVDC) system, and thermal power plants. The paper (Djamel *et al.* 2016) described the behavior of a wind farm integrated into the electrical power system and the effect of this energy on the different grid parameters such as the voltage, the load flow, and the frequency. Besides, a unified power flow controller was proposed to insert at the transmission system for improving the voltage profile. The work in (Wu *et al.* 2016) studied the impacts of increased photovoltaic (PV) installation capacity in two locations in Taiwan concerning both steady-state and dynamic performances. A charged system search algorithm was used for determining the optimal PV installed capacity at chosen buses, considering the need to minimize transmission loss and voltage variation. The impact of PV low-voltage ride-through capability on system dynamic performance was also analyzed in the work. A granular approach for investigating the impacts of very high PV generation penetration was presented in (Cheng *et al.* 2015). The study was to predict the impacts of increasing levels of PV power generation when it reached a very high penetration level.

In this paper, the authors present a research study on the application of the PSS/E software to model and simulate the 110kV transmission network in Binh Dinh province, Vietnam in the current period with the integration of the large-scale wind and solar power plants. Based on that model, operational failure scenarios for wind and solar power plants are proposed to simulate, analyze, and evaluate the stability of the 110kV grid in Binh Dinh province. The dynamic models of the Phuong Mai 3 wind power plants with a capacity of 21MW, the Fujiwara solar power plant with a peak capacity of 50MWp, and the Cat Hiep solar power plant with a peak capacity of 49.5MWp are set up in the PSS/E software to examine operational parameters such as voltage and frequency in dynamic analysis mode of the grid. The simulation results for the worst possible situations for wind and solar power plants show that the 110kV transmission network in Binh Dinh province, Vietnam remains stable to continue supplying power to the loads.

2. Background and Methodology

2.1 Description of a transmission network in Vietnam

The 110kV transmission network in Binh Dinh province, Vietnam consists of 14 substations, 301 kilometers of the transmission line, and 8 small and medium hydropower plants, including Vinh Son 66MW, Vinh Son 5 28MW, Tra Xom 20MW, Ken Loi Ha 6MW, Nuoc Xang 12.5MW, Van Phong 6MW, Tien Thuan 9.5MW, Dinh Binh 9.9MW. These hydropower plants have partly provided additional capacity for Binh Dinh province. The slack buses of the network are the 220kV substations including Quy Nhon, Phu My, Phuoc An substations. The single diagram of the 110kV power network of Binh Dinh province, Vietnam is shown in Fig. 1. The capacity of each load is characterized by variations at all times of day operation and changes according to the rules of each load substation. Therefore, in this paper, it is assumed that the load level of 80% of the rated capacity of the substations is applied to simulate the operation modes of the 110kV grid in Binh Dinh province, Vietnam. In addition, the parameters of lines, substations, and other power plants of the grid are also given in Table 1 and Table 2.

Table 1
The nominal capacity of substations.

Substation name	No.	Nominal capacity (MVA)
An Nhon	2	2×25
Don Pho	1	1×25
Dong Da	1	1×63
Hoai Nhon	2	2×25
Long My	2	40+25
My Thanh	1	1×40
Nhon Hoi	2	40+63
Nhon Tan	2	2×25
Phu Cat	2	2×25
Phu My	2	40+25
Phuoc Son	1	1×25
Quy Nhon 2	2	2×40
Tam Quan	2	40+25
Tay Son	1	1×40
Quy Nhon	2	2×40

Table 2
The specifications of 110 kV lines.

No.	Transmission line	No.	S (mm2)	L (km)
1	Vinh Son 5 - Tra Xom	1	AC-185	7.7
2	Tam Quan - Hoai Nhon	1	AC-185	17.65
3	Vinh Son - Hoai Nhon	1	AC-185	46.923
4	Vinh Son 5 - Phu My	1	AC-240	43.61
5	Tra Xom - Don Pho	1	AC-185	41.1
6	Cat Hiep - Phu Cat	1	AC-185	6.5
7	Nhon Tan - Don Pho	1	AC-185	29.513
8	Nhon Hoi - Phuong Mai 3	1	AC-185	12.31
9	Hoai Nhon - Phu My	1	AC-185	24.49
10	Phu My - My Thanh	1	AC-185	21.27
11	My Thanh - Phu Cat	1	AC-185	32.42
12	Phu Cat - An Nhon	1	AC-185	16.60
13	An Nhon - Quy Nhon 220	1	AC-185	12.67
14	Quy Nhon 220 - Quy Nhon 2	2	AC-240	9.95
15	Quy Nhon 220 - Phuoc Son	1	AC-240	13.24
16	Phuoc Son - Nhon Hoi	1	AC-240	13.75
17	Quy Nhon 220 - Long My	1	AC-185	5.67
18	Long My - Song Cau	1	AC-185	20.50
19	Nhon Hoi - Fujiwara	1	AC-185	6.5
20	Dong Da - Nhon Hoi	1	AC-185	13.2
21	Quy Nhon 220 - Dong Da	1	AC-185	13.2
22	Quy Nhon 220 - Phuoc An	1	AC-400	5.747
23	Dong Da - Cang Quy Nhon	1	AC-185	6.2
24	Phuoc An - An Nhon	1	AC-185	10.543
25	Phuoc An - Nhon Tan	1	AC-185	9.6

2.2 Network modeling using PSS/E software

The presence of the Phuong Mai 3 wind power plant with a total capacity of 21MW including 6 wind turbines, the Fujiwara solar power plant with a peak capacity of 50MWp, and the Cat Hiep solar power plant with a peak capacity of 49.5MWp have reduced 120MW of capacity taken from the power supply system. As a result, Binh Dinh Province has in part proactively reduced the amount of pure electricity and contributed to minimizing environmental impacts on human life.

The Phuong Mai 3 wind power station has a general model of type 3 wind turbine. The system is based on a doubly-fed induction generator (DFIG) as shown in Fig. 2, in which the turbine can be pitch-regulated. The AC/DC/AC converters namely Rotor-Side Converter (RSC) and Grid-Side Converter (GSC) are connected between the rotor terminal and the grid. The generator stator winding is directly coupled to the grid, and the power converter in the rotor circuit allows for independent control of generator torque and flux. To be able to provide fast active and reactive power control over a wide range of generator speeds, the control system of the Phuong Mai 3 wind power plant uses the WECC (Kaloi *et al.* 2016; Khoa *et al.* 2022; Muller *et al.* 2002). In addition, the wind turbines of the Phuong Mai 3 power station have a terminal voltage of 690V, consist of 6 pairs of poles, and have a power factor of 0.95. At each wind turbine, its output voltage is stepped up to 22kV, then to 110kV network via a 40MVA transformer to connect to the 110kV network in Binh Dinh province.

In the wind power plant, the wind turbine model is established to satisfy the following mathematical equations:

The aerodynamic torque is as in Eq. (1):

$$T_m = \frac{P_m}{\omega_t} \tag{1}$$

The mechanical power is as in Eq. (2):

$$P_m = \frac{1}{2}\rho S C_P(\lambda,\beta) v_{\text{wind}}^3 \tag{2}$$

in which ω_t is the mechanical speed, ρ is the air density, S is the blade swept area, $C_P(\bullet)$ is the performance coefficient, λ is the tip speed ratio, β is the blade pitch angle, and v_{wind} is the wind speed.

The electric generator used in this case is a Wound Rotor Induction Generator (WRIG) with the stator and rotor windings. Its parameters are given in Table 3. Moreover, its model is established in the *d-q* reference frame to satisfy the following mathematical equations (Lin *et al.* 2020; Xu *et al.* 2018; Yang *et al.* 2012):

The voltage equations as in Eq. (3):

$$\begin{aligned} u_{ds} &= R_s i_{ds} - \omega_s \lambda_{qs} + \frac{d}{dt}\lambda_{ds} \\ u_{qs} &= R_s i_{qs} + \omega_s \lambda_{ds} + \frac{d}{dt}\lambda_{qs} \\ u_{dr} &= R_r i_{dr} - (\omega_s - \omega_r)\lambda_{qr} + \frac{d}{dt}\lambda_{dr} \\ u_{qr} &= R_r i_{qr} + (\omega_s - \omega_r)\lambda_{dr} + \frac{d}{dt}\lambda_{qr} \end{aligned} \tag{3}$$

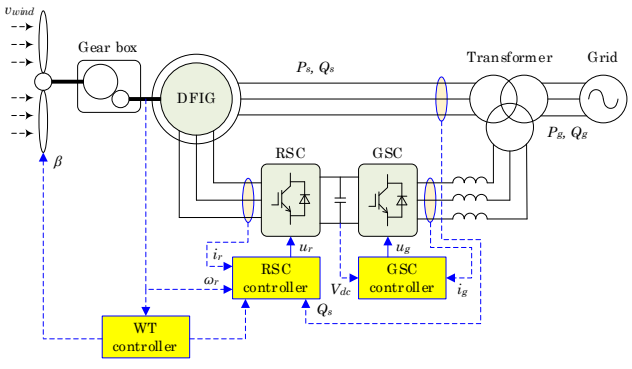

Fig. 2 The principle layout of the DFIG-based wind turbine system

Table 3
The specifications of Phuong Mai 3 wind turbine

Specification name	Parameter
Label	Siemens-Gamesa
Type	DFIG
Model	SG 3.4-132
Stator connection	Δ
Rotor connection	Y
Nominal voltage	690V
Nominal frequency	50Hz
Nominal speed	1120r.p.m
Maximum speed	1800r.p.m
Nominal capacity	3465kW
Short-circuit power	3200kW
Power factor	0.88
Number of poles	6
Inertia moment	300kgm^2

in which subscripts s and r express the stator and rotor quanta, respectively. Subscripts d and q express the d- and q-axis components, respectively; ω_s is the electrical angular speed of the grid voltage; R is the resistance; u, i and λ are the voltage, current, and flux, respectively; $\omega_r = n_p\omega_m$ is the rotor angular frequency, where ω_m is rotor mechanical speed and n_p is the number of pole pairs.

The flux equations as in Eq. (4):

$$\begin{aligned}\lambda_{ds} &= (L_{ls}+L_m)i_{ds}+L_m i_{dr} = L_s i_{ds}+L_m i_{dr}\\ \lambda_{qs} &= (L_{ls}+L_m)i_{qs}+L_m i_{qr} = L_s i_{qs}+L_m i_{qr}\\ \lambda_{dr} &= (L_{lr}+L_m)i_{dr}+L_m i_{ds} = L_r i_{dr}+L_m i_{ds}\\ \lambda_{qr} &= (L_{lr}+L_m)i_{qr}+L_m i_{qs} = L_r i_{qr}+L_m i_{qs}\end{aligned} \quad (4)$$

where L, L_l and L_m are self-inductance, leakage inductance, and mutual inductance, respectively.

The electromagnetic torque equation as in Eq. (5):

$$T_{em} = \frac{3}{2}n_p(i_{qs}\lambda_{ds} - i_{ds}\lambda_{qs}) \quad (5)$$

The instantaneous stator and rotor active power equations as in Eq. (6) (Xu *et al.* 2018):

$$\begin{aligned}P_s &= -\frac{3}{2}\omega_s\left(\lambda_{qs}i_{ds}-\lambda_{ds}i_{qs}\right)\\ P_r &= -\frac{3}{2}\left(\omega_s-\omega_r\right)\left(\lambda_{qr}i_{dr}-\lambda_{dr}i_{qr}\right)\end{aligned} \quad (6)$$

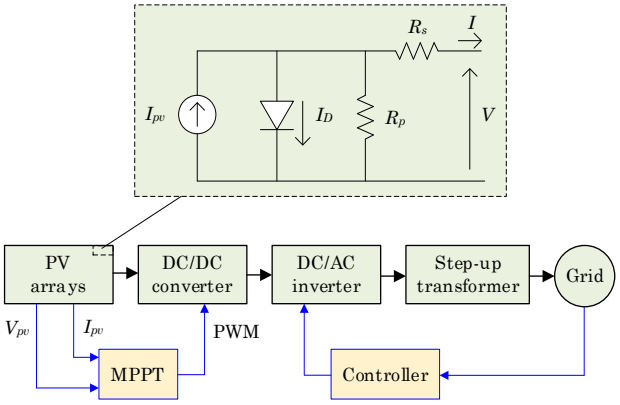

Fig. 3 Block diagram of grid-connected PV system

Table 4
The specifications of the polycrystalline solar module

Specification name	Parameter
Maximum power at STC (P_{max})	320W
Optimum operating voltage (V_{mp})	37.1V
Optimum operating current (I_{mp})	8.63A
Open circuit voltage (V_{oc})	45.6V
Short circuit current (I_{sc})	9.14A
Module efficiency	16.5%
Operating module temperature	-40 °C to +85 °C
Maximum system voltage	1500VDC (IEC)
Maximum series fuse rating	20A
Power tolerance	0/+5W

On the PSS/E software simulation tool, the panels of the Fujiwara solar power plant and the Cat Hiep solar power plant are modeled by SUNTECH panels with a peak power capacity of 282.5Wp, open-circuit DC voltage of 43.92VDC. The power output of the panels reaches its maximum of around 39VDC (Wang *et al.* 2020; Wattana *et al.* 2022). The panels are connected in series with a DC voltage of 1000VDC and a total capacity of more than 200kW per series. Using the inverter to convert DC to AC and synthesize series with a capacity of about 12.5MW, increase the voltage from 600V to 22kV through a 15MVA transformer. After that, they are transferred to a 63MVA transformer to convert the voltage from 22kV to the 110kV grid in Binh Dinh province, Vietnam. In this work, the block diagram of the grid-connected PV system is used to model the solar panel in Cat Hiep and Fujiwara solar power plants as shown in Fig. 3. The control components of grid-connected PV system consist of the maximum power point tracking and the control system of the DC/AC inverter (Hamdan *et al.* 2019; Li *et al.* 2020).

The following fundamental equations are represented to describe its terminal I-V characteristic as in Eq. (7):

$$I = I_{pv} - I_0\left[\exp\left(\frac{V+R_sI}{aV_t}\right)-1\right]-\frac{V+R_sI}{R_p} \quad (7)$$

where $V_t = N_skT/q$ is the thermal voltage of the module with k is Boltzmann's constant, I_{pv} is the photocurrent, I_0 is the diode saturation current, a is the diode ideality factor, T is the temperature of PV cell in Kelvin, N_s is the module voltage, R_s and R_p are equivalent series and parallel resistances, respectively as shown in Fig. 3.

Modeling of PV modules implies, formulating a mathematical model which provides trajectory fitments (I-V and PV curves) as given in the real datasheet of the solar power plants studied in this paper. The equations governing photocurrent and diode saturation current are stated in Eq. (8) and Eq. (9):

$$I_{pv} = \left(I_{pv,n}+K_I\Delta_T\right)\frac{G}{G_n} \quad (8)$$

$$I_0 = \frac{I_{sc,n}+K_I\Delta_T}{\exp\left(\frac{V_{oc,n}+K_V\Delta_T}{aV_t}\right)-1} \quad (9)$$

where $V_{oc,n}$ is the nominal open-circuit voltage, $I_{sc,n}$ is the nominal short circuit current, $I_{pv,n}$ (A) is the light generated current, $\Delta_T = T - T_n$ (T and T_n being the actual and nominal temperatures [K]), G (W/m^2) is the irradiation on the device surface, G_n is the nominal irradiation, K_V is the open circuit voltage-temperature coefficient, K_I is the short circuit current-temperature coefficient defined at STC and supplied by the manufacturers (Rauschenbach 1980; Villalva *et al.* 2009).

The I-V characteristic obtained from Eq. (7) shows constant current source and constant-voltage source regions. The P-V curve marks three notable points, i.e. short-circuit, open-circuit, and peak power point also called the maximum power point (MPP). This MPP value is influenced by given conditions of temperature and irradiance. The specification parameters of the polycrystalline solar module of two solar power plants are given in Table 4. Using Eq. (7), the maximum power value P_{mp} is calculated as in Eq. (10):

$$P_{mp} = V_{mp}\left[I_{pv} - I_0\left(\exp\left(\frac{V_{mp} + R_s I_{mp}}{aV_t} \right) - 1 \right) - \frac{V_{mp} + R_s I_{mp}}{R_p} \right] \quad (10)$$

3. Simulation Results and Discussion

The generating power capacity of wind power plants and solar power plants during their operation depends mainly on primary energy sources, while these sources are difficult to predict accurately (Cheng *et al.* 2015; Djamel et al. 2016). In addition, the influence of these power plants can significantly change the power flow on the grid when large dynamics occur, which makes the National Load Dispatch Centre (NLDC) facing many difficulties in the process handler (Cabrera-Tobar *et al.* 2016; Du *et al.* 2018; Mahela *et al.* 2016). Based on the grid modeling on the PSS/E software established above, scenarios related to wind and solar power plants are assumed to study the stability of the 110kV grid in Binh Dinh province, Vietnam.

3.1 The impact on the steady-state operation mode

In order to evaluate the impact of the wind power and solar power plants on the 110kV power network in this work, three cases of steady-state operation modes are investigated including: *Case 1:* The network without the wind power and solar power plants; *Case 2:* The network integrated the wind power and solar power plants which are operated in a voltage control mode; and *Case 3*: The network integrated the wind power and solar power plants which are operated in a unity power factor.

The simulation results of the three case studies which are carried out in the PSS/E software are shown in Table 5. As shown in Table 5, the bus voltages in the network are given. It shows that the bus voltages are within acceptable limits. The Phuong Mai 3 wind power plant and the Fujiwara solar power plant are connected to the grid at the bus Nhon Hoi via two 110kV transmission lines. Thus, the bus voltage of Nhon Hoi in the last case is higher than in the first case. Similarly, the Cat Hiep solar power plant is connected to the grid at the bus Phu Cat via the 110kV parallel transmission line; therefore, the bus voltage of Phu Cat in the last case is also higher than the first case.

Table 5
The bus voltage of three case studies

No.	Bus name	Voltage (%)		
		Case 1	Case 2	Case 3
1	An Nhon	96.614	97.383	96.564
2	Don Pho	98.883	98.951	98.844
3	Dong Da	95.891	96.865	95.836
4	Hoai Nhon	97.491	97.621	97.403
5	Long My	97.042	97.351	96.825
6	My Thanh	96.133	97.489	96.517
7	Nhon Hoi	94.603	97.415	95.155
8	Nhon Tan	96.513	96.859	96.354
9	Phu Cat	95.278	98.328	96.415
10	Phu My	97.609	97.917	97.519
11	Phuoc Son	95.792	97.348	95.928
12	Quy Nhon 2	96.768	97.131	96.536
13	Tam Quan	96.461	96.499	96.352
14	Tay Son	97.185	97.385	97.086
15	Quy Nhon	97.335	97.697	97.104

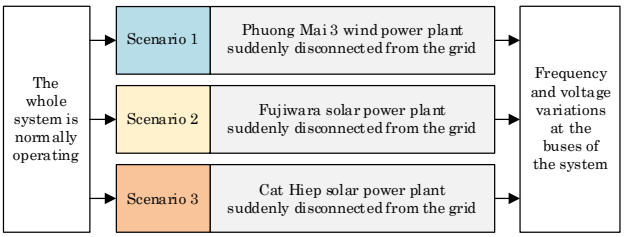

Fig. 4 Diagram for a short description of three scenarios

3.2 The impact on transient stability mode

Large disturbances are often caused by short circuits in power systems. They are usually triggered by some initial fault and then spread over the system due to combined effect of many reasons such as malfunctioning or improper operation of equipment, human faults, lack of appropriate information, etc. (Lin *et al.* 2020; Liu *et al.* 2020; Wattana *et al.* 2022). However, the 110kV power transmission network includes a wind power plant and two solar power plants which are integrated to the network. The research objective of this paper is to investigate the impact of the three power plants on the network; therefore, three typical fault scenarios for the operation are assumed to analyze and evaluate the frequency and voltage variations of the power network as shown in Fig. 4.

Three scenarios are described, simulated, and analyzed in detail as follows:

Scenario 1: Phuong Mai 3 wind power plant suddenly disconnected from the grid.

When the inverter of the grid-connected wind power plant detects a problem such as a voltage sag event with a permissible magnitude and duration, it will be disconnected from the grid. Therefore, in this scenario, assuming the Phuong Mai 3 wind power plant is generating a peak capacity of 21MW, it is suddenly separated from the grid in a period of 30sec from 5sec to 35sec. This resulted in the Phuong Mai 3 wind power plant being suddenly completely separated from the grid. The other elements on the grid are working normally during the period of investigation. The results of simulating voltage variation of neighboring buses of the Phuong Mai 3 wind power plant are shown in Fig. 5a. The load buses considered here are adjacent buses of the Phuong Mai 3

wind power plant, including Dong Da, Nhon Hoi, Phuoc Son, Phuong Mai 3, and Quy Nhon. During the time the system lost the power generated from the Phuong Mai 3 wind power plant, the voltage at some neighboring buses decreased but not significantly. Because it is near to the slack bus of the system, the voltage of the Quy Nhon bus has a very small variation and stabilizes it during the time of failure. The other buses as shown in Fig. 5a have voltage amplitude decreased in about 30sec during the fault of the Phuong Mai 3 wind power plant completely separated from the grid. Up to 35sec, the Phuong Mai 3 wind power plant is assumed to return to normal operation and connected to the grid to maintain 21MW of generating power as the original model. During this period, due to the action of the voltage controllers of the hydropower plants, the bus voltages will vary and reach the voltage value as in normal mode before happening out the fault. The simulation results shown in Fig. 5a show that when there is a sudden complete loss of the Phuong Mai 3 wind power plant, it does not affect the voltage stability of the 110kV Binh Dinh grid.

In terms of frequency stability of the 110kV Binh Dinh power grid when the sudden and complete outage of the Phuong Mai 3 power substations as the first scenario is also studied, analyzed, and evaluated in this paper. The results of the frequency variation of the grid are also recorded and shown in Fig. 5b. The dynamic models of the power substations are also incorporated into their models in the PSS/E software. At the time of 5sec, the Phuong Mai 3 wind power plant is generated into the grid with a peak capacity of 21MW but it is suddenly separated from the grid, so the frequency of the grid variation in the direction of decrease is lower than the value of 50Hz. However, owing to the frequency controls in the power plants' dynamic models, the grid frequency variation is quickly extinguished and stabilized at the 50Hz frequency. Similarly, at the time of 35sec, when the Phuong Mai 3 wind power plant is reconnected and generated an amount of power as normal mode, the frequency of the grid also tended to increase higher than the value of 50Hz, but the frequency variation is also quickly damped due to the frequency controller in dynamic models of power plants. Thus, the frequency is still maintained at 50Hz as shown in Fig. 5b.

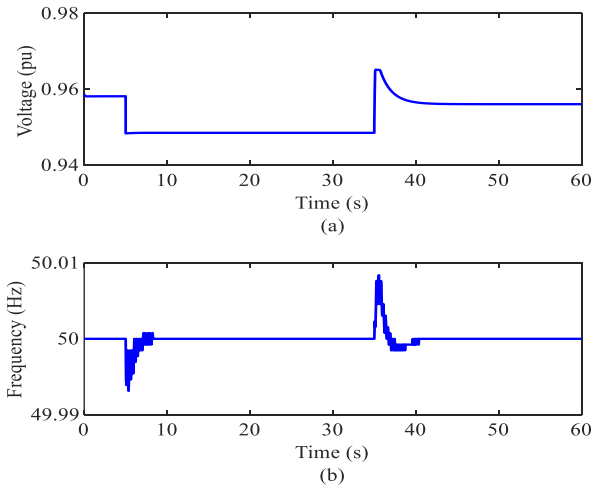

Fig. 5 Voltage and frequency variations at the Nhon Hoi bus of Scenario 1: (a) Voltage variation, (b) Frequency variation

Scenario 2: Fujiwara solar power plant suddenly disconnected from the grid

The second scenario is assumed that the Fujiwara solar power plant is generating the maximum power of 50MW but it is suddenly completely obscured by clouds in 30sec from 5sec to 35sec, which leads to its power transferring to the grid being completely lost. From 35sec, the Fujiwara solar power substation is back to the normal operation mode. The other elements on the grid are normal activities during the period of investigation. According to the current grid's structure diagram, the power supply in Dong Da, Nhon Hoi, and Phuoc Son substations is mainly supplied by the Quy Nhon substation. The Fujiwara solar power plant and the Phuong Mai 3 wind power plant share an amount of generated power to supply loads in this area. Therefore, when clouds completely cover the Fujiwara solar power plant, it also partly affects the voltage of neighboring buses. Simulation results of voltage variation at buses on the 110kV grid in Binh Dinh province of the second scenario are shown in Fig. 6a.

The process of losing the amount of generated power of the Fujiwara solar power plant due to the cloud cover from 5sec to 35sec caused the voltage at some buses on the Binh Dinh grid to decrease. According to the results in Fig. 6a, at the Nhon Hoi bus, the voltage sag is almost with the voltage amplitude decreased from 0.956pu to 0.948pu because the Fujiwara solar power plant is connected to the grid at Nhon Hoi bus. Therefore, when the loss power amount of 50MW is generated from the Fujiwara solar power plant, the system source must supply power to the load at the Nhon Hoi bus. This makes the voltage sag deeply during the transmission process, leading to a more sag in the voltage at the Nhon Hoi bus. At the same time, the voltage at the Quy Nhon substation is also decreased with a low amplitude during the fault. At the time of 35sec, the Fujiwara solar power plant is returned to normal work and continued to generate a power amount equal to 50MW as before it was not completely covered by clouds. According to the result in Fig. 6a, the bus voltages increase again and become stable at the initial voltage amplitude.

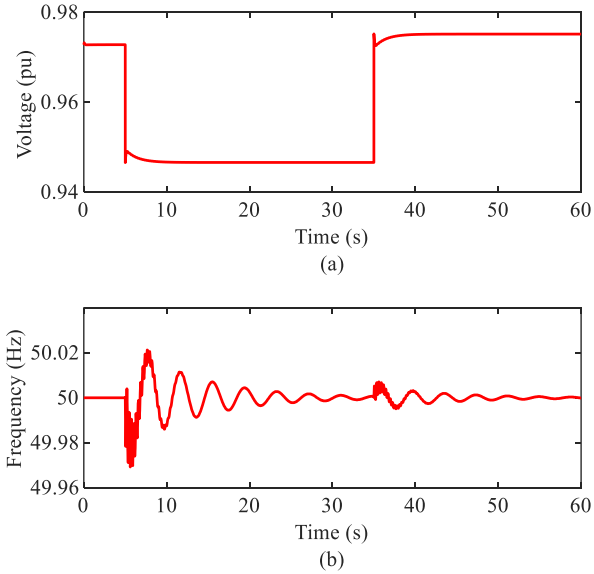

Fig. 6 Voltage and frequency variations at the Nhon Hoi bus of Scenario 2: (a) Voltage variation, (b) Frequency variation

Besides investigating voltage variation at buses on the Binh Dinh grid, the frequency variation of the grid under the second scenario is also simulated and analyzed. The results of the frequency variation of the grid due to the cloud covering the Fujiwara solar power plant, leading to the loss of 50MW are being generated to the grid as shown in Fig. 6b. According to these simulation results, the frequency variation of the grid is negligible, the frequency value is still within the permissible limits of around 50Hz. Therefore, the loss of the Fujiwara solar power plant due to completely cloud cover does not greatly affect the stability of the 110kV grid in Binh Dinh province.

Scenario 3: Cat Hiep solar power plant suddenly disconnected from the grid.

For the third scenario, a similar incident in the second scenario is the sudden loss of 49.5MW of capacity is being generated from the Cat Hiep solar power plant due to clouds completely obscuring the system of panels at the plant. This causes a sudden loss of generating capacity from the Cat Hiep solar power plant in the period from 5sec to 35sec. After the clouds passed, the Cat Hiep solar power plant returned to normal operation and continued to generate power into the grid from the time of 35sec. Simulation results of voltage variations at neighboring buses of the Cat Hiep solar power plant are shown in Fig. 7a. The simulation results of voltage variation in Fig. 7a show that the voltage at neighboring buses of the Cat Hiep solar power plant is decreased when the Cat Hiep solar power plant is completely obscured by clouds as in the third scenario. The Phu Cat bus is the position that the Cat Hiep solar power plant is connected to has the most decreased voltage amplitude (down from 0.987pu to 0.956pu) compared to the remaining buses. In addition, based on the simulation results as shown in Fig. 7a, the bus voltages quickly stabilize and reach the set value when the fault sequence occurs as in the third scenario at the time the Cat Hiep solar power plant suffers clouds are completely obscured at 5sec and at the time the Cat Hiep solar power plant is connected back to the network at the time of 35sec.

The frequency variation of the grid under the third scenario is also collected and analyzed in this case. Results of frequency variation at the buses due to the cloud covering the Cat Hiep solar power plant completely, leading to the loss of the amount of 49.5MW of power generated to the grid as shown in Fig. 7b. This result shows that trying to lose the Cat Hiep solar power plant due to completely cloud coverage at 5sec and being connected back to the grid at the time of 35sec does not greatly affect the frequency of the 110kV grid in Binh Dinh province. This variation is insignificantly small, the frequency values of the grid at that time variation within the permissible range and is quickly maintained up to 50Hz.

Based on the simulation results of the three scenarios above, the synthetic result for comparison between those scenarios is presented in Table 6. The frequency deviation and minimum voltage are determined from the results. The frequency deviations of three fault scenarios are 0.018% for Scenario 1, 0.058% for Scenario 2, and 0.036% for Scenario 3. Therefore, the frequency variations of the three scenarios are within the acceptable limit in the operating condition of the power system. Besides, the minimum voltages are also determined in the last column of Table 6. The voltage variations for the three scenarios are also within the acceptable limit.

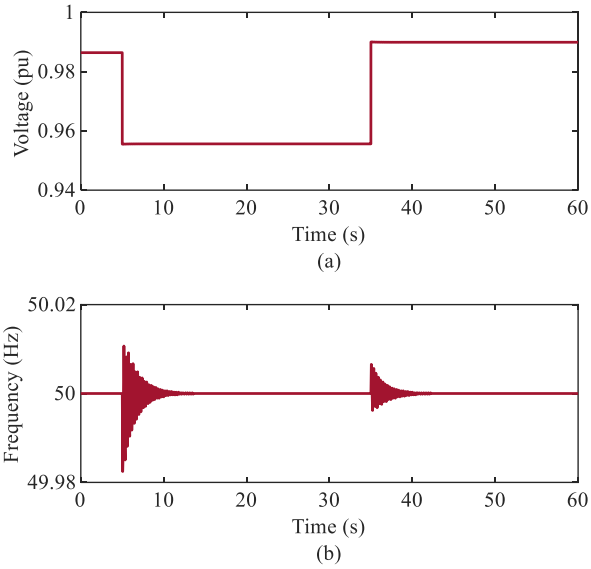

Fig. 7 Voltage and frequency variations at the Phu Cat bus of Scenario 3: (a) Voltage variation, (b) Frequency variation

Table 6
The synthetic result for comparison between three scenarios

Fault scenario no.	Type of power plant	Reduced power (MW)	Frequency deviation (%)	Minimum voltage and Bus name
1	Wind	21	0.018	0.948pu (Nhon Hoi)
2	Solar	50	0.058	0.946pu (Nhon Hoi)
3	Solar	49.5	0.036	0.955pu (Phu Cat)

4. Conclusion

The paper has researched modeling the 110kV transmission network in Binh Dinh province, Vietnam with the integration of wind and solar power plants on the PSS/E software. Dynamic models of the large-scale renewable power plants are integrated with simulation diagrams to carry on research results. Three possible scenarios for the large-scale renewable power plants including Phuong Mai 3 wind power plant, Fujiwara solar power plant, and Cat Hiep solar power plant are investigated in this paper to analyze and evaluate their effects on voltage and frequency variation of the 110kV transmission network in Binh Dinh province. The voltage and frequency variations at the buses on the grid were used for impact analysis of the large-scale renewable power plants on the system. The simulation results show that when there are problems during the operation of these power plants, voltage, and frequency variations at the buses on the network are still negligible and the system still ensures stability to continue operating normally.

Funding: This research is funded by the Ministry of Education and Training, Vietnam under the grant number CT 2022.07.DNA.08.

References

Abbas, S. R., Kazmi, S. A. A., Naqvi, M., Javed, A., Naqvi, S. R., Ullah, K., Khan, T. R., & Shin, D. R. (2020). Impact analysis of large-scale wind farms integration in weak transmission grid from technical perspectives. *Energies*, 13(20), 5513; doi: 10.3390/en13205513

Ameur, A., Berrada, A., Loudiyi, K., & Aggour, M. (2019). Analysis of renewable energy integration into the transmission network. *The Electricity Journal*, 32(10), 106676; doi: 10.1016/j.tej.2019.106676

Cabrera-Tobar, A., Bullich-Massagué, E., Aragüés-Peñalba, M., & Gomis-Bellmunt, O. (2016). Review of advanced grid requirements for the integration of large scale photovoltaic power plants in the transmission system. *Renewable and Sustainable Energy Reviews*, 62, 971-987; doi: 10.1016/j.rser.2016.05.044

Cheng, D., Mather, B. A., Seguin, R., Hambrick, J., & Broadwater, R. P. (2015). Photovoltaic (PV) impact assessment for very high penetration levels. *IEEE Journal of Photovoltaics*, 6(1), 295-300; doi: 10.1109/JPHOTOV.2015.2481605

Dai, L. V., Khoa, N. M., & Quyen, L. C. (2020). An Innovatory Method Based on Continuation Power Flow to Analyze Power System Voltage Stability with Distributed Generation Penetration. *Complexity*, 2020, 8037837; doi: 10.1155/2020/8037837

Denholm, P., Hand, M. (2011). Grid flexibility and storage required to achieve very high penetration of variable renewable electricity. *Energy Policy*, 39(3), 1817-1830; doi: 10.1016/j.enpol.2011.01.019

Djamel, L., Zohra, M., & Selwa, F. (2016). Influence of the wind farm integration on load flow and voltage in electrical power system. *International Journal of Hydrogen Energy*, 41(29), 12603-12617; doi: 10.1016/j.ijhydene.2016.04.230

Du, E., Zhang, N., Hodge, B. M., Wang, Q., Kang, C., Kroposki, B., & Xia, Q. (2018). The role of concentrating solar power toward high renewable energy penetrated power systems. *IEEE Transactions on Power Systems*, 33(6), 6630-6641; doi: 10.1109/TPWRS.2018.2834461

Fant, C., Schlosser, C. A., & Strzepek, K. (2016). The impact of climate change on wind and solar resources in southern Africa. *Applied Energy*, 161, 556-564; doi: 10.1016/j.apenergy.2015.03.042

Hamdan, I., Maghraby, A., & Noureldeen, O. (2019), Stability improvement and control of grid-connected photovoltaic system during faults using supercapacitor. *SN Applied Sciences*, 1, 1687; doi: 10.1007/s42452-019-1743-2

Hu, J., Liu, X., Shahidehpour, M., Xia, S. (2021). Optimal Operation of Energy Hubs With Large-Scale Distributed Energy Resources for Distribution Network Congestion Management. *IEEE Transactions on Sustainable Energy*, 12(3), 1755-1765; doi: 10.1109/TSTE.2021.3064375

Impram, S., Nese, S. V., & Oral, B. (2020). Challenges of renewable energy penetration on power system flexibility: A survey. *Energy Strategy Reviews*, 31, 100539; doi: 10.1016/j.esr.2020.100539

Jasemi, M., Adabi, F., Mozafari, B., Salahi, S. (2016). Optimal operation of micro-grids considering the uncertainties of demand and renewable energy resources generation. *International Journal of Renewable Energy Development*, 5(3), 233-248; doi: 10.14710/ijred.5.3.233-248

Kaloi, G. S., Wang, J., & Baloch, M. H. (2016). Active and reactive power control of the doubly fed induction generator based on wind energy conversion system. *Energy Reports*, 2(2016), 194-200; doi: 10.1016/j.egyr.2016.08.001

Kim, E. H., Kim, J. H., Kim, S. H., Choi, J., Lee, K. Y., & Kim, H. C. (2011). Impact analysis of wind farms in the Jeju Island power system. *IEEE Systems Journal*, 6(1), 134-139; doi: 10.1109/JSYST.2011.2163017

Khoa, N. M., & Tung, D. D. (2018). Locating fault on transmission line with static var compensator based on phasor measurement unit. *Energies*, 11(9), 2380; doi: 10.3390/en11092380

Khoa, N. M., Tung, D. D., & Dai, L. V. (2022). Experimental study on low voltage ride-through of DFIG-based wind turbine. *International Journal of Electrical and Electronic Engineering & Telecommunications*, 11(1), 1-11, 2022; doi: 10.18178/ijeetc.11.1.1-11

Li, L., Li, H., Tseng, M. L., Feng, H., & Chiu, A. S. F. (2020). Renewable energy system on frequency stability control strategy using virtual synchronous generator. *Symmertry*, 12, 1697; doi: 10.3390/sym121016

Lin, C., Song, Y., Zhao, J., Liang, G., Qiu, J. (2020). Assessing the impacts of large-scale offshore wind powerin Southern China, Energy Conversion and Economics, John Wiley & Sons Ltd.

Liu, R., Yao, J., Wang, X., Sun, P., Pei, J., & Hu, J. (2020). Dynamic stability analysis and improved LVRT schemes of DFIG-based wind turbines during a symmetrical fault in a weak grid. *IEEE Transactions on Power Electronics*, 35(1), 303-318; doi: 10.1109/TPEL.2019.2911346

Mahela, O. P., & Shaik, A. G. (2016). Comprehensive overview of grid interfaced wind energy generation systems. *Renewable and Sustainable Energy Reviews*, 57, 260-281; doi: 10.1016/j.rser.2015.12.048

Muller, S., Deicke, M., & De Doncker, R. W. (2002). Doubly fed induction generator systems for wind turbines. *IEEE Industry Applications Magazine*, 8(3), 26-33; doi: 10.1109/2943.999610

Rauschenbach, H. (1980). Solar cell array design handbook-The principles and technology of photovoltaic energy conversion, Springer.

Ullah, Z., Baseer, M. (2022). Operational planning and design of market-based virtual power plant with high penetration of renewable energy sources. *International Journal of Renewable Energy Development*, 11(3), 620-629; doi: 10.14710/ijred.2022.44586

Villalva, M. G., Gazoli, J. R., & Ruppert-Filho, E. (2009). Comprehensive approach to modeling and simulation of photovoltaic arrays. *IEEE Transactions on Power Electronics*, 24(5), 1198-1208; doi: 10.1109/TPEL.2009.2013862

Wang, L., Qiao, T., Zhao, B., Zeng, X., & Yuan, Q. (2020). Modeling and parameter optimization of grid-connected photovoltaic systems considering the low voltage ride-through control. *Energies*, 13(15), 3972; doi: 10.3390/en13153972

Wattana, B., Aungyut, P. (2022). Impacts of solar electricity generation on the Thai Electricity Industry. *International Journal of Renewable Energy Development,* 11(1), 157-163; doi: 10.14710/ijred.2022.41059

Wu, Y. K., Ye, G. T., & Shaaban, M. (2016). Analysis of impact of integration of large PV generation capacity and optimization of PV capacity: Case studies in Taiwan. *IEEE Transactions on Industry Applications*, 52(6), 4535-4548; doi: 10.1109/TIA.2016.2594283

Xu, D., Blaabjerg, F., Chen, W., & Zhu, N. (2018). Advanced control of doubly fed induction generator for wind power systems, John Wiley & Sons

Yang, L., Xu, Z., Ostergaard, J., Dong, Z. Y., Wong, K.P. (2012). Advanced control strategy of DFIG wind turbines for power system fault ride through. *IEEE Transactions on Power Systems*, 27(2), 713-722; doi: 10.1109/TPWRS.2011.2174387